High-Throughput Screening of Mg-Functionalized Metal-Organic Frameworks for Hydrogen Storage near Room Temperature

Yamil J. Colón,[†‡] David Fairen-Jimenez,[† §‡] Christopher E. Wilmer,[†] and Randall Q. Snurr[†]*

[†]Department of Chemical and Biological Engineering, Northwestern University, 2145 Sheridan Road, Evanston, IL, 60208, USA

[§]Department of Chemical Engineering and Biotechnology, University of Cambridge, Pembroke Street, Cambridge CB2 3RA, United Kingdom

*To whom correspondence should be addressed. E-mail: snurr@northwestern.edu

1

ABSTRACT: The hydrogen storage capabilities of 18,383 porous crystalline structures possessing various degrees of Mg functionalization and diverse physical properties were assessed through combined grand canonical Monte Carlo (GCMC) and quantum mechanical approaches. GCMC simulations were performed for pressures of 2 and 100 bar at a temperature of 243 K. Absolute uptake at 100 bar and deliverable capacity between 100 bar and 2 bar were calculated. Maximum absolute and deliverable gravimetric capacities were 9.35 wt% and 9.12 wt % respectively. Volumetrically, absolute and deliverable capacities were 51 g/L and 30 g/L respectively. In addition, the results reveal relationships between hydrogen uptake and the physical properties of the materials. We show that the introduction of an optimum amount of Mg alkoxide to increase the isosteric heat of adsorption is a promising strategy to improve hydrogen uptake and delivery near ambient temperature.

Hydrogen has long been proposed as a possible alternative to fossil fuels for powering vehicles.[1,2] It is particularly attractive because it is non-toxic and its oxidation product is water. However, hydrogen storage has proved challenging. The U.S. Department of Energy (DOE) has calculated that 4 kg or 44,000 L of gaseous H_2 are needed to provide enough energy to fuel a typical automobile.[3] This is translated to system requirements of 7.5 wt% and 70 g/L of H_2 at a minimum temperature of 243 K and a maximum pressure of 100 bar.[4] The challenge is to design H_2 storage systems that efficiently and safely store H_2 in a realistic volume and that allow it to be easily extracted at reasonable pressures and temperatures. Several technologies are being developed to meet these goals, such as high-pressure gas and cryogenic tanks.[1,3] In addition, materials that chemisorb H_2, such as metal hydrides,[2,5] or physisorb H_2, such as metal-organic frameworks (MOFs),[6] are under intensive investigation.

In general, metal hydrides are capable of high uptake but bind hydrogen too tightly because the H_2 molecule is dissociated. The strong binding energy and slow H-H recombination kinetics make the release of hydrogen difficult. On the other hand, physisorption systems have the opposite problem: they bind H_2 too weakly, and although they are able to release it efficiently, their adsorption capacity is very limited, especially at room temperature.

MOFs are a widely studied class of H_2 storage materials.[7,8] They are porous, crystalline materials comprised of metal *nodes* connected by organic *linkers*. The great variety of possible nodes and linkers offers the opportunity to design and tune MOFs for particular applications. They possess large internal surface areas, up to 7100 m^2/g, which provide outstanding adsorption capacities.[9-12] Related materials, crystalline porous aromatic frameworks (PAFs), have also been reported recently.[13-15] PAFs have a diamond-like structure where tetrahedral carbon atoms act as nodes, linked by aromatic linkers. However, H_2 uptake in MOFs and PAFs at ambient temperature has thus far been low because the heats of adsorption have been too low. The highest experimental uptake values reported to date for room temperature hydrogen storage are *ca.* 2.3 wt% and 12.1 g/L (values refer to excess uptake).[7,8,16]

Recently, metal alkoxide functionalization of the organic linkers has been demonstrated experimentally as a possibility to tune the surfaces of MOFs.[17,18] This approach has been shown to be promising for hydrogen storage because the positive charge of the metal interacts favorably with the H_2 quadrupole, increasing the capacity of the materials.[19-24] In preliminary work, we studied the interaction of various metal alkoxide groups (Li, Be, Mg, Mn, Fe, Ni, Cu, and Zn) with H_2 using MP2 and M06 quantum mechanical calculations.[24,25] Of these metals, we found magnesium to be best for H_2 storage and delivery, in agreement with other studies.[26,27] Magnesium alkoxide functional groups significantly improved storage capacities near room temperature in several structures relative to their unfunctionalized analogues. Magnesium's advantages, relative to other metals, are twofold. First, the H_2 binding energy is high, but not so high that it retains the H_2 at low pressure, which would reduce the deliverable capacity. Second, the H_2 binding energy is relatively constant as loading increases.

In this work, we aimed to determine whether there exists a plausible configuration of Mg alkoxide functional groups in a porous material that would meet the DOE H_2 storage targets. Using recently developed structure generating algorithms,[28] we created a library of 18,383 hypothetical structures with varying degrees of Mg alkoxide functionalization and a diverse range of textural properties. Figure 1

3

illustrates how the structures were generated. The resulting materials were screened for H_2 uptake at 243 K at 2 and 100 bar using grand canonical Monte Carlo (GCMC) simulations, where the H_2 interactions with the Mg alkoxide groups were modeled using *ab initio* quantum mechanics calculations.[24] From the GCMC simulations, we obtained the amount of H_2 adsorbed at 2 and 100 bar as well as the isosteric heats of adsorption (Q_{st}). The deliverable capacity was calculated by subtracting the amount of H_2 adsorbed at 2 bar from the amount adsorbed at 100 bar. From this data, gravimetric and volumetric H_2 uptake (absolute and deliverable) were then related to various material properties.
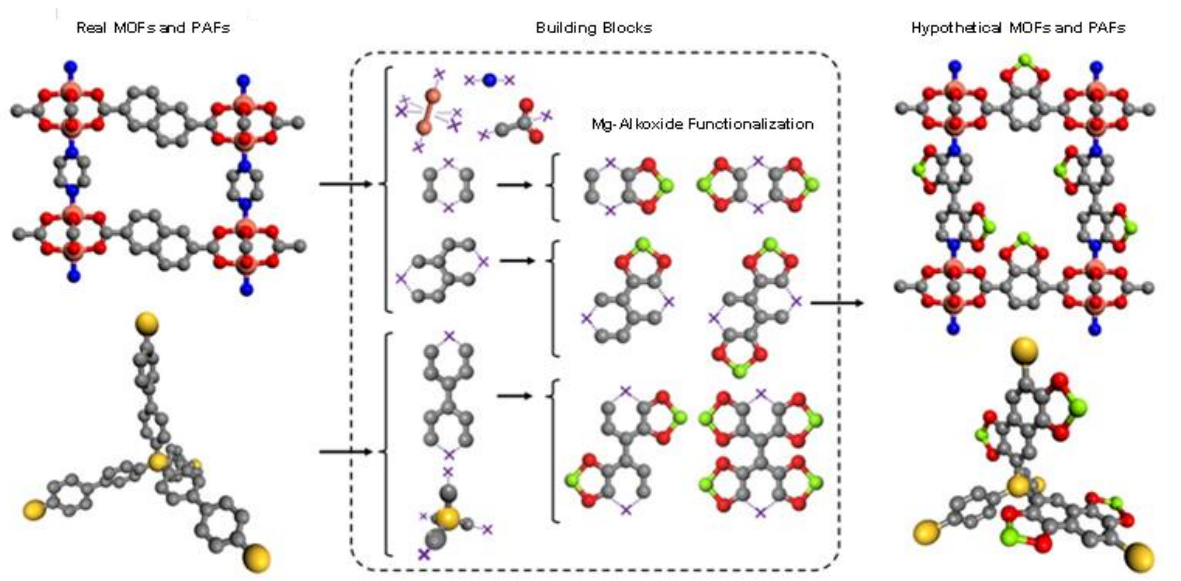
Figure 1. Our approach deconstructs known porous crystals into modular components (i.e. building blocks) that can be systematically reassembled into new, hypothetical materials. Before the building blocks are assembled into crystal structures, they can be functionalized to varying degrees with Mg alkoxide groups. Hydrogen atoms have been omitted for clarity, and gray, red, pink, blue, yellow, and green spheres represent carbon, oxygen, copper, nitrogen, carbon corners, and magnesium atoms, respectively. Purple x's represent sites where building blocks can be connected to each other.

Results and Discussion

In a gas storage application, it is critical not only to obtain a high capacity at high pressure, but also to be able to release the adsorbed gas efficiently at lower pressure.[25,29] In a scenario where two structures have similar uptake at 100 bar but differing uptake at 2 bar (due to different adsorbent/adsorbate interaction strengths), the deliverable capacity of the structures will also be different. If the interactions are too strong, the structure will saturate at lower pressures and this can harm the deliverable capacity. If they are too weak, the structure may not saturate even at 100 bar but a higher deliverable capacity may be achieved. This is illustrated in Figure S1. Results in the literature indicate that to improve hydrogen uptake in MOFs at 100 bar and near room temperature, it is necessary to increase the adsorbent/adsorbate interactions beyond what is observed in unfunctionalized MOFs.

While much work has focused on the gravimetric targets, in a typical automotive application, limited volume for the storage tank is the more critical problem, making the volumetric adsorption capacity particularly important. For the 18,383 structures generated, Figure 2 shows their ranking based on their H_2 volumetric deliverable capacities at ambient temperature (black). The deliverable gravimetric capacities are also shown in red. The maximum H_2 deliverable capacities obtained at 243 K are 30 g/L and 9.1 wt%. In general, those materials that excel in one uptake metric do not do as well in the other. For example, the material with the highest volumetric deliverable capacity (i.e., 30 g/L) falls short in the gravimetric capacity (i.e., 4.6 wt%). Further, Figure 2 reveals that the materials among the top 3 % in volumetric capacity show large differences in terms of gravimetric capacities, ranging from 2.5 to 6.0 wt%.
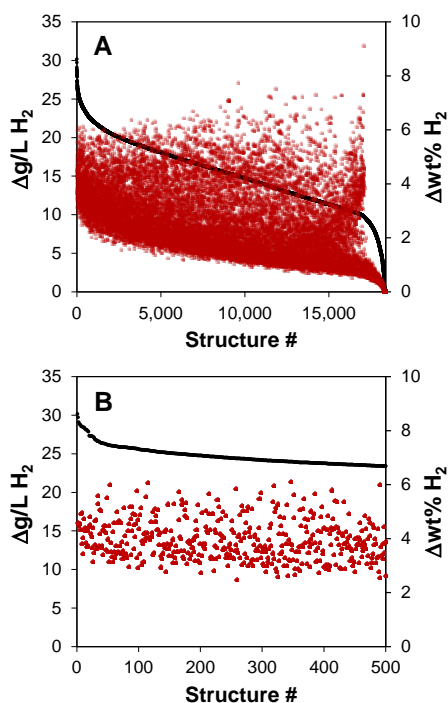
Figure 2. Ranking of MOF structures in terms of deliverable volumetric capacity (black points). Red points represent the corresponding deliverable gravimetric capacities. Lower panel shows the top 500 structures (i.e., top 3 %) in volumetric capacity.

To analyze these differences, we studied the relationships between the H_2 storage capacities and the material properties. The structures generated show significant diversity and possess a wide range of structural characteristics. Generated structures range from 0 to 0.98 in helium void fraction; 0 to 10,776 m^2/g in surface area; 0 to 7.7 mmol/cm^3 in Mg alkoxide density; and 0 to 30.66 kJ/mol in isosteric heat of adsorption at 2 bar. Figures 3, S4, and S5 show the results obtained for absolute and deliverable H_2 uptake in both gravimetric and volumetric quantities. The gravimetric capacity increases with increasing void fraction, while the volumetric capacity has a maximum at around 0.75 void fraction (Figure 3). There is a broad dispersion of capacities for any given void fraction. This is because the capacities depend not only on the void fraction, but on multiple additional factors such as degree of functionalization and Q_{st}. The results show that the highest volumetric capacities are localized at 2.5 mmol/cm^3 Mg alkoxide density and 17 kJ/mol Q_{st}. For gravimetric uptake, increasing Mg functionalization and higher Q_{st} increase the uptake at most void fractions (Figure 3). However, the materials with the very highest gravimetric uptake, surprisingly, have low Mg density and thus low

6

Q_{st}. For both volumetric and gravimetric uptake, Figures 3, S4, and S5 indicate a clear correlation between degree of Mg functionalization and Q_{st}, which shows that Mg alkoxide functionalization can be used to optimize the isosteric heat of adsorption and, in turn, H_2 uptake capacities.
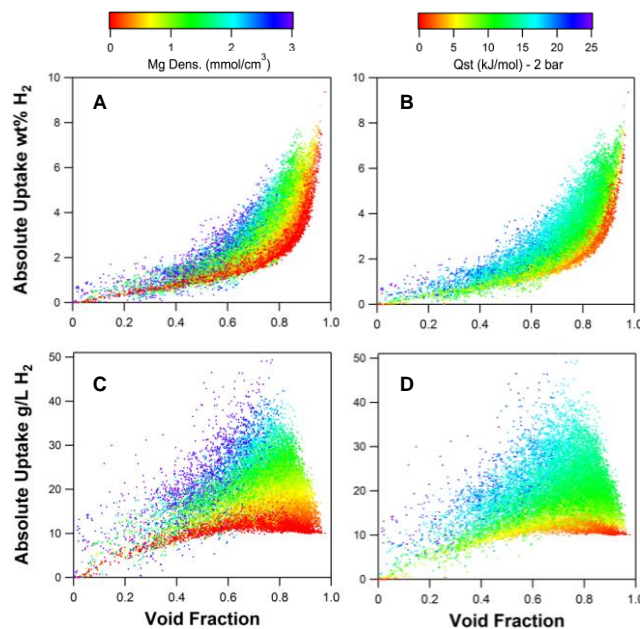
Figure 3. Absolute gravimetric (top) and volumetric (bottom) H_2 uptake versus void fraction obtained from simulated isotherms at 243 K and 100 bar on 18,383 different materials. Colors indicate the Mg alkoxide density (left), and the isosteric heat of adsorption at 2 bar (right). Note that each point represents a single material. Alkoxide densities higher than 3 mmol/cm^3 have been represented using the last color (i.e., purple).

The balance between gravimetric and volumetric deliverable capacities is explored in Figure 4. The structures with the highest gravimetric deliverable capacity, which are those with low Mg density, perform poorly in terms of the volumetric capacity. On the other hand, structures with high volumetric deliverable capacity (those with Mg density *ca.* 2.5 mmol/cm^3) have gravimetric deliverable capacities around 4 wt%, which is not bad, although it is less than the current targets. It is also interesting to note that structures with intermediate Mg densities possess intermediate volumetric deliverable capacities.

There is a fundamental limitation that prevents a material from having large volumetric and gravimetric deliverable capacities simultaneously. For an optimal gravimetric capacity, the material should have a low framework density. The insertion of relatively heavy Mg metals compared with C, O

and H atoms does not improve this characteristic. On the other hand, for an optimal volumetric capacity there is a balance between void fraction and material density, confirming our previous findings, where the highest H_2 uptake corresponded to materials with not-so-high porosity.[30] In this case, the insertion of Mg metals only causes a small reduction in the pore volume that is compensated by the higher interaction and Q_{st}.
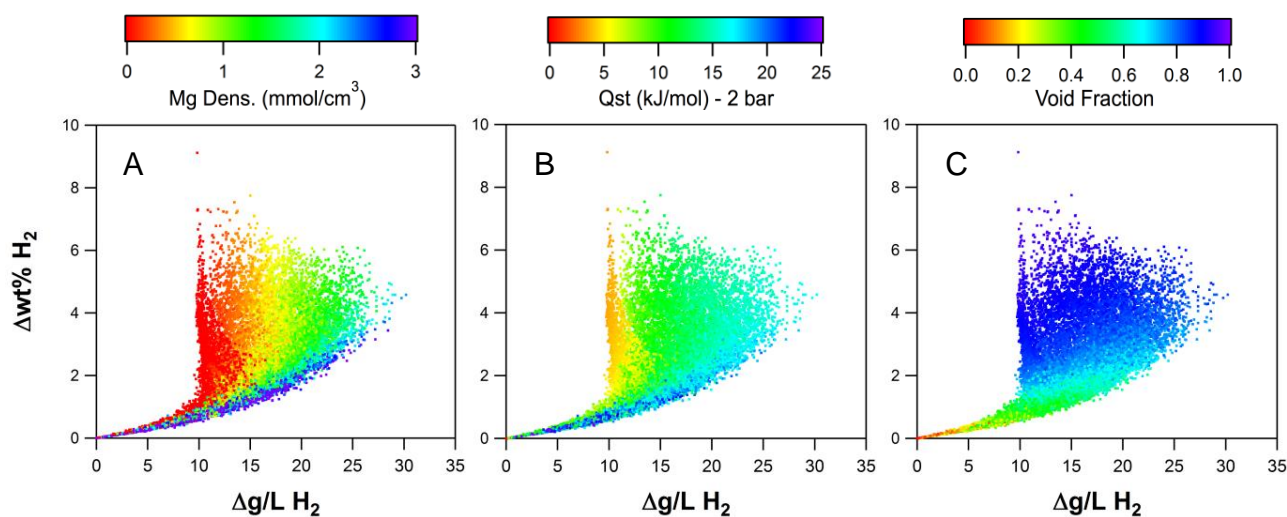
Figure 4. Deliverable gravimetric versus volumetric capacity obtained from simulated isotherms at 243 K and 2 and 100 bar. Colors indicate the Mg alkoxide density (left), the isosteric heat of adsorption at 2 bar (center), and void fraction (right).

Although deliverable capacities are of critical importance for vehicular storage applications, the absolute capacities at a single pressure are related to the material characteristics in a more straightforward manner. Figure 5 shows the relation between absolute and deliverable capacities and the influence of Mg density, and Figure S6 includes the effects of Q_{st} and void fraction. In order to maximize the absolute volumetric uptake at 100 bar, high values of Mg density (*ca.* 2.5 mmol/cm^3) and Q_{st} (*ca.* 17 kJ/mol) are necessary. However, as mentioned above, higher Q_{st} increases adsorption at low pressures, hence harming the deliverable capacity and causing the large differences between absolute and deliverable capacity observed in Figures 5 and S6. It is interesting to note that structures that possess optimum Mg densities and Q_{st} for gravimetric deliverable capacity (i.e., low Mg densities and Q_{st} values) show less difference between absolute and deliverable uptake, both for gravimetric and

volumetric. For example, the best gravimetric structure shows 9.35 *vs.* 9.12 wt. % of absolute and deliverable capacity, respectively, with 0.0 mmol/cm^3 and 3.2 kJ/mol of Mg density and Q_{st}, respectively. In the case of volumetric, small differences between absolute and deliverable are extended up to *ca.* 17 g/L (absolute), with Mg densities and Q_{st} *ca.* 0.0 mmol/cm^3 and 6 kJ/mol, respectively.Figure S6 also reveals that the structures with the highest void fractions deviate to a lesser degree when comparing the absolute and deliverable amounts despite high Mg functionalization and, consequently, high Q_{st}. With a high void fraction not only the absolute but also the deliverable quantities may be increased.
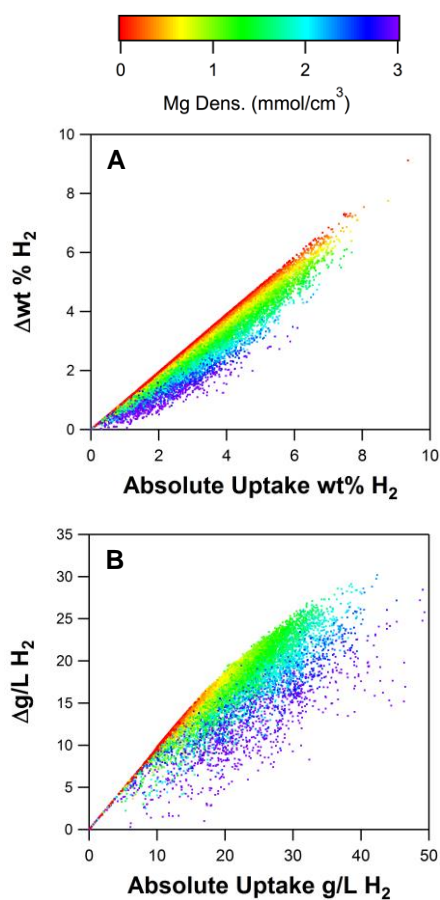
Figure 5. Deliverable capacity vs. absolute uptake at 100 bar at 243 K, gravimetric (top) and volumetric (bottom). Colors indicate the Mg alkoxide density.

In order to obtain MOFs and PAFs with large pore volumes and surface areas, one can increase the length of the organic linkers. However, this increases the possibility of catenation.[31] Network

catenation occurs when two or more independent, identical networks are entangled, partially filling each other's pores. Catenation results in a decrease of the void fraction and the pore volume. Figures 6 and S7 show the influence of catenation on the absolute uptake as a function of the volumetric and gravimetric surface area, respectively. Figure S8 shows the influence of catenation on deliverable uptake as a function of the void fraction. The gravimetric uptake (Figure 6, top) reveals two distinct regions composed of different types of materials. The materials comprising the upper region with a negative slope are those which have the possibility to be catenated due to their high pore volume, but are not. The materials in the lower region with a positive slope are the catenated materials or those that due to their low porosity do not have this possibility. Figure 6 shows that the different uptake values observed within each region are a consequence of the Mg functionalization. Within one region, and for similar volumetric surface areas, materials with higher Mg density show higher absolute uptake. This result suggests a path for optimizing future H_2 storage materials. Namely, through the development of new synthetic techniques to prevent catenation in structures that otherwise would be catenated, higher absolute uptake capacities may be achieved.

For absolute volumetric uptake (Figure 6, lower panels), the catenation effect is not as clear, but the effect of Mg density is evident. Interestingly, the apparent slope of each region increases with Mg functionalization. Plotting absolute uptake (gravimetric and volumetric) versus gravimetric surface area reveals similar trends to those observed for volumetric uptake versus volumetric surface area (Figure S7).
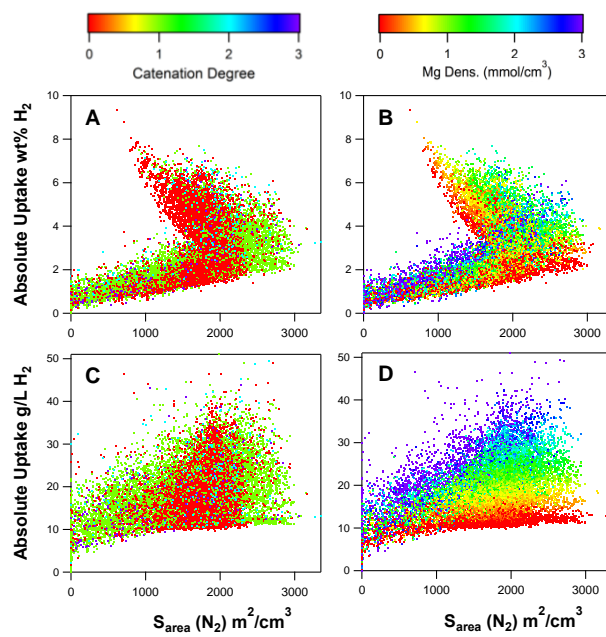
Figure 6. Gravimetric and volumetric H$_2$ absolute uptake at 100 bar and 243 K as a function of the volumetric surface area. Colors indicate the catenation degree (*left*) and Mg alkoxide density (*right*).

In this work, we screened 18,383 new hypothetical structures with varying degrees of Mg alkoxide functionalization for possible H$_2$ storage applications and revealed important structure/property relationships. In addition, the work has suggested strategies for synthesizing new material targets that, if achieved, would represent improvements over current hydrogen storage materials. Large-scale, high-throughput computational screening of the adsorption properties of materials allows us to explore what could be the ultimate limits of these types of porous media.

Methods

All 18,383 structures based on MOF and PAF precursors were generated using crystal enumeration algorithms previously reported.[28] The lists of nodes and linkers are provided in the Supporting Information (SI). Figure 1 illustrates how the generation of the new structures takes place. Existing porous crystals are broken up into their building blocks. The organic linkers can then be functionalized to various degrees with Mg alkoxides, providing new building blocks for the crystal generation. The

metal or carbon nodes and linkers, described in Figures S2 and S3, are then combined to form new hypothetical crystals.

Interactions between H_2 molecules and the Mg alkoxide functionalization were modeled using a Morse plus Coulomb potential. The potential was parameterized previously using quantum chemical calculations at the MP2/6-311+G** level of theory with counterpoise corrections to correct for basis set superposition errors (BSSE).[24,32] Coulomb interactions were calculated using Ewald sums with partial charges on the alkoxide atoms[24] and the Darkrim-Levesque[33] model for H_2, which places charges of +0.468 on the H nuclei and a -0.936 charge on the center of mass.

H_2 interactions with all other framework atoms were described using Lennard-Jones (LJ) potentials, with parameters for the framework atoms taken from the Universal Force Field (UFF).[34] H_2 LJ parameters were taken from the Michels-Degraaff-Tenseldam model.[35] H_2/H_2 interactions were modeled using a LJ + Coulomb potential using the LJ parameters from the Michels-Degraaff-Tenseldam model and charges from the Darkrim-Levesque model. All cross terms were calculated using Lorentz Berthelot mixing rules. A cutoff of 12.0 Å was used for the LJ interactions. All framework atoms were held fixed throughout the simulations, and the H_2 molecules were assumed to be rigid.

Grand canonical Monte Carlo (GCMC) simulations were carried out using our in-house code RASPA.[36] Simulations were performed in cells with sufficient repeat units such that all edges were greater than 24 Å. In each simulation, 20,000 cycles were performed for system equilibration and another 20,000 were performed to calculate ensemble averages. In a cycle, an average of N moves was performed, where N is the number of molecules in the system. Monte Carlo moves were translation, rotation, insertion, deletion, and random reinsertion at a new position in the framework. Simulations were performed at pressures of 2 and 100 bar at a temperature of 243 K. Q_{st} was calculated from fluctuation theory during the GCMC simulation.[37]

Surface areas (SA) were computed by rolling a N_2 probe of 3.681 Å over the framework atoms.[38]

He void fractions for the structures were calculated using Widom insertions.[39]

AUTHOR INFORMATION

Corresponding Author

*snurr@northwestern.edu

Author Contributions

‡Y.J.C. and D.F-J. contributed equally to this work.

ACKNOWLEDGMENT

REFERENCES

(1)   Jorgensen, S. W. *Current Opinion in Solid State and Materials Science* **2011**, *15*, 39.
(2)   David, W. I. F. *Faraday Discussions* **2011**, *151*, 399.
(3)   DOE(US) 2012.
(4)   U.S., D. O. E.;
http://www1.eere.energy.gov/hydrogenandfuelcells/storage/pdfs/targets_onboard_hydro_storage.pdf

Vol. 2013.
(5)   B. Sakintuna; F. L. Darkrim; M., H. *Int. J. Hydrogen Energy* **2007**, *32*, 1121.
(6)   Rowsell, J. L. C.; Yaghi, O. M. *Angew. Chem. Int. Ed.* **2005**, *44*, 4670.
(7)   Murray, L. J.; Dinca, M.; Long, J. R. *Chem. Soc. Rev.* **2009**, *38*, 1294.
(8)   Suh, M. P.; Park, H. J.; Prasad, T. K.; Lim, D.-W. *Chemical Reviews* **2011**, *112*, 782.
(9)   Farha, O. K.; Yazaydin, A. O.; Eryazici, I.; Malliakas, C. D.; Hauser, B. G.; Kanatzidis, M. G.; Nguyen, S. T.; Snurr, R. Q.; Hupp, J. T. *Nature Chemistry* **2010**, *2*, 944.
(10) Farha, O. K.; Eryazici, I.; Jeong, N. C.; Hauser, B. G.; Wilmer, C. E.; Sarjeant, A. A.; Snurr, R. Q.; Nguyen, S. T.; Yazaydın, A. Ö.; Hupp, J. T. *Journal of the American Chemical Society* **2012**, *134*, 15016.
(11) Furukawa, H.; Ko, N.; Go, Y. B.; Aratani, N.; Choi, S. B.; Choi, E.; Yazaydin, A. O.; Snurr, R. Q.; O'Keeffe, M.; Kim, J.; Yaghi, O. M. *Science* **2010**, *329*, 424.

(12) Sarkisov, L. *Advanced Materials* **2012**, *24*, 3130.

(13) Ben, T.; Ren, H.; Ma, S.; Cao, D.; Lan, J.; Jing, X.; Wang, W.; Xu, J.; Deng, F.; Simmons, J. M.; Qiu, S.; Zhu, G. *Angewandte Chemie International Edition* **2009**, *48*, 9457.

(14) Lan, J.; Cao, D.; Wang, W.; Ben, T.; Zhu, G. *The Journal of Physical Chemistry Letters* **2010**, *1*, 978.

(15) Ben, T.; Pei, C.; Zhang, D.; Xu, J.; Deng, F.; Jing, X.; Qiu, S. *Energy & Environmental Science* **2011**, *4*, 3991.

(16) Lim, W.-X.; Thornton, A. W.; Hill, A. J.; Cox, B. J.; Hill, J. M.; Hill, M. R. *Langmuir* **2013**, *29*, 8524.

(17) Mulfort, K. L.; Farha, O. K.; Stern, C. L.; Sarjeant, A. A.; Hupp, J. T. *J. Am. Chem. Soc.* **2009**, *131*, 3866.

(18) Himsl, D.; Wallacher, D.; Hartmann, M. *Angew. Chem. Int. Ed.* **2009**, *48*, 4639.

(19) Lochan, R. C.; Head-Gordon, M. *Physical Chemistry Chemical Physics* **2006**, *8*, 1357.

(20) Yang, Q. Y.; Zhong, C. L. *J. Phys. Chem. B Lett.* **2006**, *110*, 655.

(21) Sun, Y. Y.; Kim, Y.-H.; Zhang, S. B. *J. Am. Chem. Soc.* **2007**, *129*, 12606.

(22) Lochan, R. C.; Khaliullin, R. Z.; Head-Gordon, M. *Inorganic Chemistry* **2008**, *47*, 4032.

(23) Dinca, M.; Long, J. R. *Angew. Chem. Int. Ed.* **2008**, *47*.

(24) Getman, R. B.; Miller, J. H.; Wang, K.; Snurr, R. Q. *J. Phys. Chem. C* **2011**, *115*, 2066.

(25) Brand, S. K.; Colón, Y. J.; Getman, R. B.; Snurr, R. Q. *Microporous and Mesoporous Materials* **2013**, *171*, 103.

(26) Tylianakis, E.; Klontzas, E.; Froudakis, G. E. *Nanotechnology* **2009**, *20*, 204030.

(27) Stergiannakos, T.; Tylianakis, E.; Klontzas, E.; Froudakis, G. E. *The Journal of Physical Chemistry C* **2010**, *114*, 16855.

(28) Wilmer, C. E.; Leaf, M.; Lee, C. Y.; Farha, O. K.; Hauser, B. G.; Hupp, J. T.; Snurr, R. Q. *Nature Chem.* **2012**, 83.

(29) Bae, Y.-S.; Snurr, R. Q. *Microporous Mesoporous Mater.* **2010**, *132*, 300.

(30) Fairen-Jimenez, D.; Colon, Y. J.; Farha, O. K.; Bae, Y.-S.; Hupp, J. T.; Snurr, R. Q. *Chemical Communications* **2012**, *48*, 10496.

(31) Rosi, N. L.; Eddaoudi, M.; Kim, J.; O'Keeffe, M.; Yaghi, O. M. *Angew. Chem. Int. Ed.* **2002**, *41*, 284.

(32) Boys, S. F.; Bernardi, F. *Mol. Phys.* **2002**, *100*, 65.

(33) Darkrim, F.; Levesque, D. *J. Chem. Phys.* **1998**, *109*, 4981.

(34) Rappé, A. K.; Casewit, C. J.; Colwell, K. S.; III, W. A. G.; Skiff, W. M. *J. Am. Chem. Soc.* **1992**, *114*, 10024.

(35) Michels, A.; Degraaff, W.; Tenseldam, C. A. *Physica* **1960**, *26*, 393.

(36) Dubbeldam, D.; Calero, S.; Ellis, D. E.; Snurr, R. Q.; 1.0 ed.; Northwestern University: Evanston, IL, 2008.

(37) Karavias, F.; Myers, A. L. *Langmuir* **1991**, *7*, 3118.

(38) Düren, T.; Bae, Y.-S.; Snurr, R. Q. *Chemical Society Reviews* **2009**, *38*, 1237.

(39) Myers, A. L.; Monson, P. A. *Langmuir* **2002**, *18*, 10261.